Available online at www.sciencedirect.com
SCIENCE DIRECT
Journal of Catalysis 228 (2004) 130–140
JOURNAL OF CATALYSIS
www.elsevier.com/locate/jcat

(*R*,*R*)-Tartaric acid on Ni(110): the dynamic nature of chiral adsorption motifs

Vincent Humblot, Sam Haq, Chris Muryn, Rasmita Raval *

The Surface Science Research Centre, Department of Chemistry, University of Liverpool, Liverpool L69 3BX, UK

Received 17 June 2004; revised 2 August 2004; accepted 17 August 2004

Available online 29 September 2004

Abstract

Nickel surfaces modified by optically active tartaric acid have been shown to be very effective in heterogeneous enantioselective hydrogenation reactions, but the performance of the catalysts is critically determined by the preparation conditions. Crucially, the enantioselective performance is linked directly to the presence of the chiral modifiers, yet little is known about the nature of the chiral adsorbate on the modified surface. Recently, model chirally modified surfaces created by the adsorption of the well-known modifier, (*R*,*R*)-tartaric acid, on a Cu(110) single crystal surface, have been shown to exhibit a variety of surface phases. In this paper, we turn from the Cu(110) surface to the Ni(110) surface, which is the metal most commonly used in the successful catalytic system. The chemical nature and orientation of the adsorbed chiral species were analysed by Fourier transform reflection absorption infrared spectroscopy (FT-RAIRS), while the two-dimensional order of the adlayer was investigated by scanning tunneling microscopy (STM). This work shows that on Ni(110), too, a complex adsorption phase diagram exists, in which different bonding, molecular forms, and orientation of the chiral molecules are adopted, from the intact biacid form at $T = 90$ K, to the singly deprotonated monotartrate form between the temperature range of 170–270 K, to the coverage-dependent behaviour at $T > 270$ K, where the doubly deprotonated bitartrate species is preferred at low coverage, while the monotartrate species is preferred at high coverages. This versatility of structural and chemical form and its delicate dependence on preparation conditions give insight into the behaviour of the real catalyst system where small changes in formulation conditions can lead to significant loss of enantiomeric excess (ee).

Keywords: Heterogeneous enantioselective catalysis; Tartaric acid adsorption; Ni(110); RAIRS; STM

1. Introduction

The synthesis of pure enantiomers underpins the chiral technologies of pharmaceutical and chemical industries, and is driven by the fact that even ppm levels of the undesired enantiomer can have catastrophic consequences in physiological applications. Although homogeneous catalytic or organic synthetic routes are currently used in industrial processes, there are strong reasons for exploring alternative heterogeneous catalytic processes, which offer easier handling, recovery, and separation. However, progress in formulating efficient heterogeneous catalysts is seriously hampered by the lack of fundamental details on the construction and operation of successful enantioselective active sites. At present, only two heterogeneous enantioselective reactions have merited much attention: the hydrogenation of β-ketoesters over supported nickel catalysts and the hydrogenation of α-ketoesters over supported platinum catalysts [1,2]. In these systems, enantioselectivity is induced at the achiral metal catalyst by first modifying it by the adsorption of chiral "modifier" molecules. Perhaps, the most notable aspect of these chiral catalytic systems is how preparation conditions, especially temperature and coverage, are strong influencers of catalytic performance.

For the nickel systems, α-amino acids and α-hydroxy acids are both successful modifiers, and the local nature of the chiral molecule at the surface is central to understand-

* Corresponding author. Fax: +44 151 794 3896.
E-mail address: raval@liv.ac.uk (R. Raval).

0021-9517/$ – see front matter
doi:10.1016/j.jcat.2004.08.023

ing the chiral influence it exerts on the reaction. Given that the complexity of a real catalytic system makes it almost impossible to extract such information, we have chosen to study a mimic of a catalytic system by adsorbing pure enantiomers of chiral molecules on a defined single crystal metal surface. In this paper, we report on the behaviour of (*R*,*R*)-tartaric acid on a Ni(110) surface. Tartaric acid (TA) is one of the most successful modifier molecules for the enantioselective hydrogenation of the simplest β-ketoester methylacetoacetate (MAA) [1]. On (*R*,*R*)-tartaric acid-modified nickel catalysts, the reaction is stereo-controlled so that the (*R*)-methyl-3-hydroxybutyrate (MHB) product is obtained in enantiomeric excess (ee) of over 90%. Conversely, on (*S*,*S*)-tartaric acid-modified surfaces, the enantioselectivity is switched to lead mainly to the (*S*)-product [3,4]. Recently, we have shown that (*R*,*R*)-tartaric acid occupies a complex phase space on Cu(110) with the details of the local adsorption entity and its self-assembly being determined critically by the adsorption conditions [5,6]. An interesting aspect of this system is that at certain points of the phase diagram, one observes the creation of extended chiral surfaces, in which the chiral molecules assemble in highly organised structures which possess growth directions that destroy all the mirror symmetry planes of the underlying metal surface [5–8]. The "handedness" created by such adsorption structures is sustained over the entire surface which are, therefore, globally chiral. Thus, chirality is bestowed at two different levels: at the local level where chiral adsorption motifs are present and at the long-range level when these units assemble into chiral two-dimensional architectures. More recently, investigations on the (*R*,*R*)-tartaric acid/Ni(111) system [9] show the formation of long-range ordered adlayers of tartrate species on Ni(111), with the two-dimensional packing, thermal stability, and molecular conformation of the modified surfaces being critically linked to the sample temperature and arrival rate of the modifier molecules at the surface.

In this paper, the chemical nature and orientation of the adsorbed (*R*,*R*)-tartaric acid species on Ni(110) were analysed as a function of coverage and temperature by Fourier transform reflection absorption infrared spectroscopy (FT-RAIRS), which is one of the most powerful surface spectroscopies for eliciting such information. We have already shown that local structure is the critical factor in controlling the expression of surface chirality [10,11] and, therefore, any fundamental understanding needs to map the nature of this structure. Our data on the (*R*,*R*)-tartaric acid/Ni(110) system show that the chiral centres of the molecule survive the adsorption process over the 90–350 K temperature range and that the detailed nature of the local adsorbate structure displays dynamic changes with coverage and temperature. A detailed adsorption phase diagram (Fig. 1), has been constructed which clearly indicates that the nature of the chiral influence that emanates from the adsorbate must be expected to change, depending on the conditions. Finally, the results obtained are compared and contrasted to the previously reported work on Cu(110) [5,6] and Ni(111) [9].

2. Experimental methods

Two ultrahigh vacuum (UHV) chambers were used in this study. The first chamber contained facilities for RAIRS, temperature-programmed desorption (TPD), low-energy electron diffraction (LEED), Auger electron spectroscopy (AES), and sample cleaning. This chamber was interfaced with a commercial Mattson 6020 FTIR spectrometer equipped with a liquid nitrogen cooled HgCdTe detector possessing a spectral range of 650–4000 cm^{-1}. RAIR spectra were collected throughout a continuous dosing regime as sample single beam infrared spectra and ratioed against a background single beam reference of the clean nickel surface. All spectra were obtained at 4 cm^{-1} resolution with coaddition of 200 scans.

The second chamber was an Omicron Vakuumphysik variable temperature-STM chamber with facilities for STM, LEED, AES, and sample cleaning. All STM experiments were carried out with the sample at room temperature. The images were acquired in constant current mode.

In each chamber, the Ni(110) crystal was cleaned by cycles of Ar^+ ion sputtering and annealing to 900 K. The surface cleanliness and ordering were monitored by AES and LEED. The nickel crystals were provided by Surface Preparation Laboratory, The Netherlands, with purity of 99.99% (4N), and alignment accuracies of 0.5 and 0.1° for the RAIRS and the STM experiments, respectively. (*R*,*R*)-Tartaric acid (99%) was obtained from Sigma-Aldrich Chemicals, and was used without any further purification. The sample was contained in a small resistively heated glass tube, separated from the main chamber by a gate valve and differentially pumped by a turbo molecular pumping system. Before sublimation, tartaric acid was outgassed at 330 K, then heated to 370 K, and exposed to the nickel crystal. During sublimation the main chamber base pressure was typically 2×10^{-9} mbar.

3. Results and discussion

3.1. Local chemical nature of the (R,R)-tartaric acid molecule

(*R*,*R*)-Tartaric acid, or L(+)-2,3-dihydroxysuccinic acid, is a chemically adaptable molecule, which can exist in at least three different forms: the neutral biacid form, the monotartrate form where one of the carboxylic acid groups is deprotonated, and the bitartrate form, where both acid groups are deprotonated producing two carboxylate functionalities. The vibrational structure for each form is different [12–14], so they may be distinguished by IR spectroscopy. For example, the presence of the carboxylate group

is signaled by the appearance of the ν_{OCO}^{asym} and the ν_{OCO}^{sym} vibrations around 1600 and 1400 cm^{-1}, respectively, while the carboxylic acid group is indicated by distinct $\nu_{C=O}$ and ν_{C-O} vibrations around 1750 and 1380 cm^{-1}, respectively [15]. The use of RAIRS with a metal surface also allows the orientation of the different functional groups of the adsorbate to be deduced by the application of dipole selection rules [16], which specify that only vibrational modes with a dynamic dipole moment change perpendicular to the surface will be observed.

Our previous work on copper [5] also yielded an IR database for the different molecular forms of TA adsorbed at the surface. Each form is well characterised by the functional groups and their IR activity. Thus, the biacid form is identified by the presence of the main IR features at 1750, 1446, 1379, 1271, and 1136 cm^{-1} assigned, respectively, to the $\nu_{C=O}$ (free biacid molecules), ν_{C-OH}^{acid}, δ_{OH}^{alc}, δ_{OH}^{acid}, and ν_{C-OH}^{alc} vibrations. The monotartrate form, where one acid group deprotonates, leads to the appearance of IR features at 1711 and 1437 cm^{-1} assigned, respectively, to the $\nu_{C=O}$ vibration of the remaining intact carboxylic group and to the ν_{OCO}^{sym} vibration of the carboxylate group. Finally, when the second acid group deprotonates to give rise to the bitartrate form, contributions from any acidic function disappear. Instead, a doublet is observed in the 1430–1410 cm^{-1} region due to the coupled oscillator system of the two carboxylate groups, while the feature at 1113 cm^{-1} (ν_{C-OH}^{alc}) dramatically increases its intensity for the bitartrate form.

Our analysis for the Ni(110) system will be mainly based on these previous results for Cu(110) [5] and compared to the recent results on Ni(111) obtained by us (this work) and others [9]. In order to facilitate the discussion, an adsorption phase diagram is shown in Fig. 1, which summarises the molecular nature and the characteristic bonding observed as a function of adsorption temperature and coverage conditions for (*R*,*R*)-TA adsorbed on Ni(110).

3.2. Low-temperature adsorption: the molecular biacid phase

Adsorption at low temperatures (90–120 K) leads to the creation of just one adsorption species on Ni(110), the undissociated biacid (Fig. 1). Data associated with this chiral adsorbate are discussed below. Figs. 2a and b show the RAIR spectra obtained with increasing coverage of (*R*,*R*)-tartaric acid on Ni(110) at 90 K. No change in the band positions from low (submonolayer, spectrum (a)) to high exposures (multilayers, spectrum (b)) is observed. All the RAIR absorption bands observed are close to the IR bands observed for solid (*R*,*R*)-tartaric acid [12], suggesting that, at low temperatures, weakly perturbed neutral biacid molecules are adsorbed on the nickel surface throughout the monolayer to multilayer regime. Table 1 shows the infrared absorption bands and assignments for crystalline tartaric acid in comparison with those for tartaric acid adsorbed on a Ni(110) surface at 90 K. There is a good agreement in the assignments of the bands between this work and those in the literature [12], as well as with the IR frequencies for (*R*,*R*)-TA multilayers adsorbed on Cu(110) [5] and Ni(111) [9] surfaces. In addition, the biacid phase is also observed at higher temperatures up to 300 K. However, here it is only present in the multilayer regime with peaks appearing at 1757, 1441, and 1135 cm^{-1} that characterise the growth of tartaric acid multilayers on the top of the monolayer initially created.

Finally, the feature at 2035 cm^{-1} present in the RAIR spectra shown in Fig. 2 is attributed to the stretching vibration of CO molecules coadsorbed on the Ni(110) surface [17,18]. From the fact that the intensity of this peak does

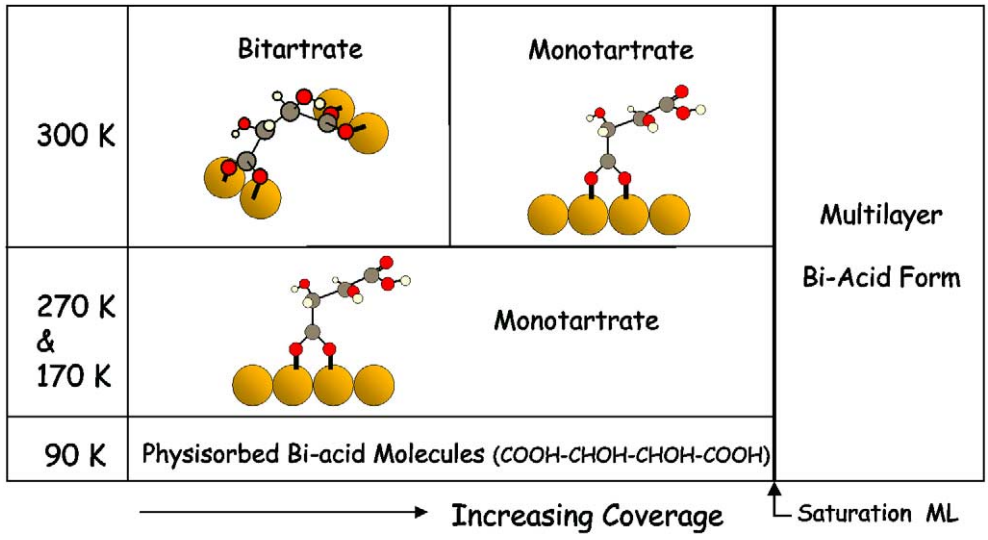

Fig. 1. Adsorption phase diagram showing the chemical nature adopted by (*R*,*R*)-tartaric acid molecules on the Ni(110) surface as a function of temperature and coverage.

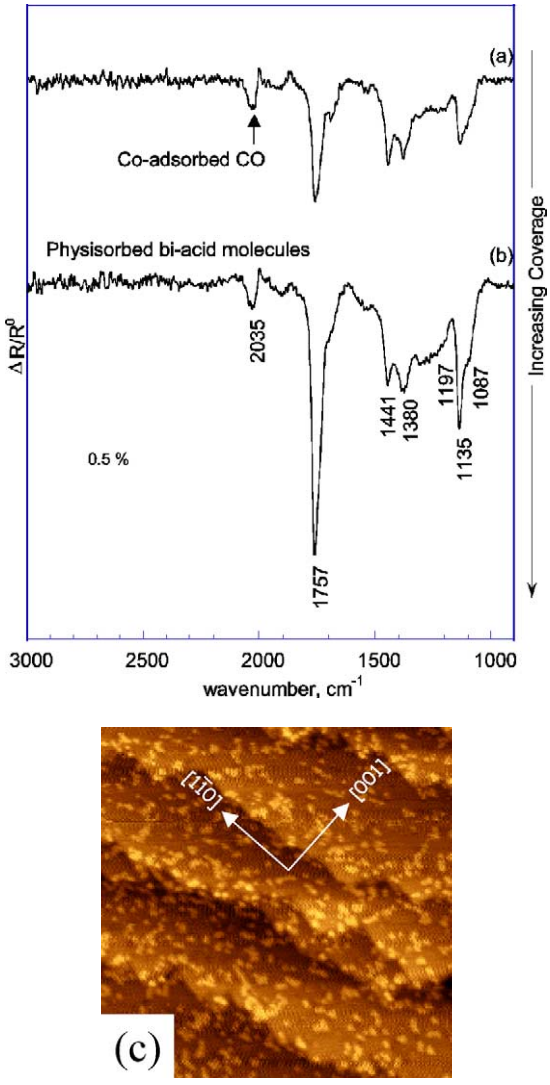

Fig. 2. RAIR spectra following the adsorption of (*R*,*R*)-tartaric acid on Ni(110) at 90 K as a function of coverage. Sublimation exposure time: (a) 3 min and (b) 12 min. (c) STM image of (*R*,*R*)-tartaric acid adsorbed on Ni(110) at 102 K, showing aggregates of physisorbed molecules, 750 × 750 Å, $V = -2.68$ V, $I = 1.0$ nA.

not change upon adsorption of tartaric acid and from the analysis of temperature-programmed desorption, it can be concluded that this low coverage of CO molecules present on the surface is due to adsorption from residual gas in the chamber and, therefore, not attributed to any cracking dissociation fragments of the adsorbed tartaric acid molecules.

No ordered overlayer LEED patterns were observed following the adsorption of (*R*,*R*)-tartaric acid on Ni(110) at 90 K. The absence of long-range ordered structures at these temperatures is also confirmed by the STM data. The STM image in Fig. 2c was recorded after initial adsorption of (*R*,*R*)-tartaric acid at 102 K on clean Ni(110), and displays no obvious order of the molecules. Instead a large number of fractal molecular aggregates with dimensions in the range of 20 to 35 Å diameters are observed.

3.3. Adsorption between 170 and 270 K: the monotartrate phase (monolayer) and the biacid phase (multilayer)

The phase diagram shown in Fig. 1 shows that the (*R*,*R*)-tartaric acid/Ni(110) system exhibits the same behaviour in the monolayer over the entire temperature range of 170 to 270 K, namely the creation of the singly deprotonated chiral monotartrate adsorption motif. Therefore, the main features of this phase are illustrated using the results obtained at 170 K. RAIR spectra (Fig. 3) following the adsorption of (*R*,*R*)-tartaric acid at 170 K on Ni(110) provide direct information on the molecular nature of the adsorbed species. At low coverage in the first layer, the IR data (Fig. 3a) reveal a weak, broad band at 1687 cm^{-1} and a sharp band at 1437 cm^{-1}. The former can be attributed to a $\nu_{C=O}$ stretching vibration of the carboxylic acid [19], and its frequency is indicative of a highly hydrogen-bonded system; the latter is a strong indicator of the ν^{sym}_{OCO} vibration for the deprotonated carboxylate group bound to the surface [15]. Therefore, we attribute this spectrum to a monotartrate species. This rationalisation is identical to that put forward for the monotartrate phase on the Cu(110) surface [5,6,20] and the general characteristics of the RAIR spectrum in Fig. 3a bear close similarities with those obtained for the monotartrate on Cu(110) and Ni(111) (Fig. 4a). The one major difference observed is the frequency and breadth of the $\nu_{C=O}$ stretching vibration, which is much broader and downshifted for the Ni(110) system, suggesting a greater degree of inter- and/or intramolecular hydrogen bonding; clearly this aspect is highly susceptible to changes in the geometric and chemical nature of the surface.

A detailed assignment of all the infrared bands observed in Fig. 3a has been made with reference to the assignments for the monotartrate species adsorbed on Cu(110) [5,6,20] and by combining the information available for the crystalline biacid phase [10] and bitartrate salts [11] (Table 1). Individual bands observed for the main functional groups of the monotartrate species, e.g., COOH, COO^-, $OH_{alcohol}$, and OH_{acid}, are indicated by the following IR bands: $\nu_{C=O}$, ν^{sym}_{OCO}, δ^{alc}_{OH}, and δ^{acid}_{OH}, and correspond to those observed for the monotartrate/Cu(110) system [5,20].

Application of the infrared metal surface selection rule [16] allows some aspects of the orientation adopted by the monotartrate adsorbate to be determined. The presence of a medium intensity ν^{sym}_{OCO} vibration at 1437 cm^{-1} and the absence of the ν^{asym}_{OCO} vibration expected in the 1550–1650 cm^{-1} region indicate that the two oxygen atoms in the carboxylate group are equidistant from the surface, leading to an inactive asymmetric stretch of the OCO^- group, but reinforcing the symmetric stretching vibration. Following the general interaction mechanism of the carboxylate functionality with metal surfaces, it is proposed that the bonding with the metal takes place via the oxygens of the carboxylate group, thus anchoring the monotartrate species to the surface. We note, however, that the intensity of the ν^{sym}_{OCO} vibration at the saturation coverage (estimated

Table 1
Characteristic vibrational bands, in cm^{-1}, and assignments for the biacid phase, the monotartrate phase, and the bitartrate phase formed by the adsorption of (*R*,*R*)-tartaric acid on Ni(110) in comparison with tartaric acid powder [12], anhydrous Rochelle salt powder [13], biacid/monotartrate/bitartrate on Cu(110) [5] and on Ni(111) (this work and [9])[a]

Assignment	TA powder [12]	Rochelle salt[b] powder [13]	RAIRS data for the biacid TA on			RAIRS data for the monotartrate phase on			RAIRS data for the bitartrate phase on		
			Cu(110) [5]	Ni(111) (this work and [9])	Ni(110) (this work)	Cu(110) [5]	Ni(111) (this work and [9])	Ni(110) (this work)	Cu(110) [5]	Ni(111) (this work and [9])	Ni(110) (this work)
$\nu_{C=O}$	1741 br,vs		1750 s	1761	1756 vs	1711 s	1692	1687 br,m			
ν_{OCO}^{asym}		1594 br,s								1602	
ν_{C-O}^{acid}	1453 br,s		1446 so	1397	1441 m						
ν_{OCO}^{sym}		1433 s 1411 s				1437 s	1427	1437 sh,m	1430 sh,s 1401 br,m	1422	1434 sh,m 1401 br,m
δ_{OH}^{alc} [c]	1375 s	1380 s 1344 w	1379 br	1380	1390 br,m	1398 w 1378 w,sh	1380	1380 sh,m 1325 br,m	1375 s	1365 1337	1370 sh,m 1325 br,s
$\delta_{OH}^{acid} + \delta_{C-H}$	1318 w 1255 m 1220 m		1271 br	1307 1212 1189	1247 br,s 1197 br,w	1338 w 1300 w 1234 m	1237 br	1247 br,s			
δ_{C-H}		1312 w 1245 vw 1211 vw					1195		1338 s 1200 w	1185	1272 sh,w
ν_{C-O}^{alc} [c]	1190 m 1134 m 1087 m	1113 w 1069 w	1136 m 1090 m	1109 1061	1135 m 1089 sh,w	1197 w 1101 m	1124	1182 br,m 1108 br,m 1089 br,m	1113 s	1108 1061	1110 sh,s
ν_{C-C}	992 w	994 w	999 vw	959					999 sh,w	954	999 sh,m

[a] s, m, w, v, br, and sh indicate strong, medium, weak, very, broad, and shoulder, respectively.
[b] Rochelle salt: $K^+Na^+[OOC–CHOH–CHOH–COO]^{2-}$.
[c] alc, alcohol.

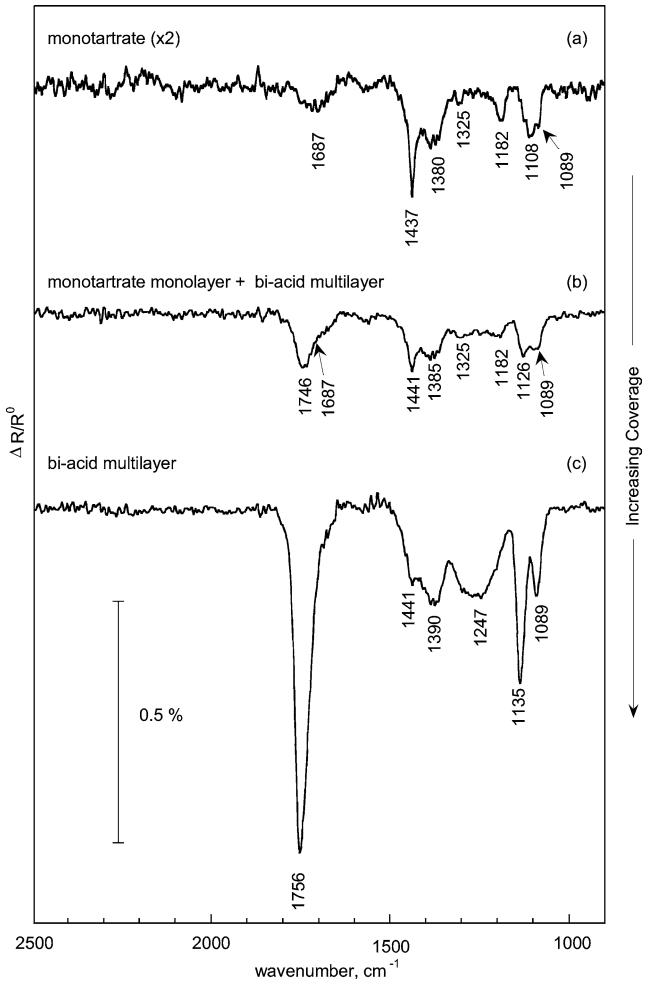

Fig. 3. RAIR spectra following the adsorption of (*R*,*R*)-tartaric acid on Ni(110) at 170 K as a function of coverage. Sublimation exposure time: (a) 4.5 min, (b) 6 min, and (c) 16.5 min.

at 0.25 ML from STM data, see below) is almost a factor of 5 lower than observed for the equivalent vibration from 0.25 ML of formate on Cu(110) and Ni(110) [21,22], implying that the plane of this group in the monotartrate species is strongly inclined toward the surface. Turning to the remaining carboxylic acid group at the other end of the molecule, the $\nu_{C=O}$ stretching vibration is observed as a broad band at 1687 cm^{-1}, showing a downshift with respect to the multilayer value at 1757 cm^{-1}, thus indicating the presence of considerable H-bonding interactions. Its relatively lower intensity compared to the Cu(110) and Ni(111) systems (Figs. 3a and 4a) suggests a greater tendency to be oriented along the surface plane. Fig. 1 shows a schematic representation of the monotartrate adsorbed to nickel atoms through both oxygens of its carboxylate group. It is important to note that the RAIRS data do not allow the precise orientation of the remaining functional groups to be determined, and, therefore, these positions in the schematic are only approximate, based on the relative intensities of the appropriate bands.

LEED and STM experiments were carried out in order to probe the two-dimensional order of the monotartrate adlayer formed at 170 K. Again, no ordered overlayer LEED structures were observed at any stage, suggesting that there is no long-range order for this adlayer. However, STM data obtained at 170 K with increasing coverage of (*R*,*R*)-tartaric acid on Ni(110) (Fig. 5) allow a description of the overlayer to be formulated. These confirm the LEED data in that no extended two-dimensional order is observed. Generally, adsorption leads to random occupation on the surface, with the monotartrate molecules imaged as white circular dots forming random 1-D molecular aggregations of single, double, triple, etc units, with a preferred growth direction along the <1–10> close-packed rows (Figs. 5a and b). Statistical profile studies of the images recorded for the isolated molecules show that the monotartrate structures occupy on average a space of $6.1 \pm 0.3 \times 4.6 \pm 0.3$ Å, with the nearest neighbour distances of 5.4 ± 0.3 Å in the <1–10> direction and 7.7 ± 0.3 Å in the <001> direction. This suggests a local (2×2) unit lattice in terms of molecular packing, but such periodicity was never observed by LEED even at monolayer saturation coverage, due to the lack of long-range order.

Alongside the monotartrate species, the presence of black troughs and white chains on the surface can also be discerned. These are due to the well-known (1×2) reconstruction of Ni(110) in the presence of hydrogen atoms, leading to removal of nickel atoms to form missing rows (black troughs) and nucleation of the Ni atoms into added rows (white chains) [23]. The presence of H-induced features is largely attributed to the first deprotonation of the tartaric acid molecules during the formation of the monotartrate species, with only a small fraction arising from background pickup. This reconstruction is of a very local nature, with single hydrogen atoms extracting Ni atoms out into Ni–H-chain-like structures [23]. In accordance with this, our STM images show the spacing between two neighbouring added rows or two neighbouring missing rows to be 7.2 ± 0.3 Å, a value that is in close agreement with the crystallographic data of 7.04 Å, i.e., twice the lattice spacing in the <001> direction. Thermal desorption experiments of the H/Ni(110) system [24,25] show three desorption states: the α-state desorbing at $\sim$ 220 K, and the β_1- and β_2-desorption states that evolve at 290 and 340 K, respectively, suggesting that coadsorbed hydrogen atoms and associated surface reconstruction can be expected to be present on our surface until 340 K. We also note that the adsorption of the monotartrate species at 170 K occurs randomly across the surface, suggesting that the coadsorption of hydrogen, and thus the reconstructions induced by it, does not play any role in the adsorption of the (*R*,*R*)-tartaric acid molecules, and that the two adsorption phases are essentially independent from each other.

Finally, once saturation coverage is reached in the monolayer, subsequent adsorption of the intact biacid molecules occurs to create multilayers on top of the monotartrate monolayer, as seen clearly in the development of charac-

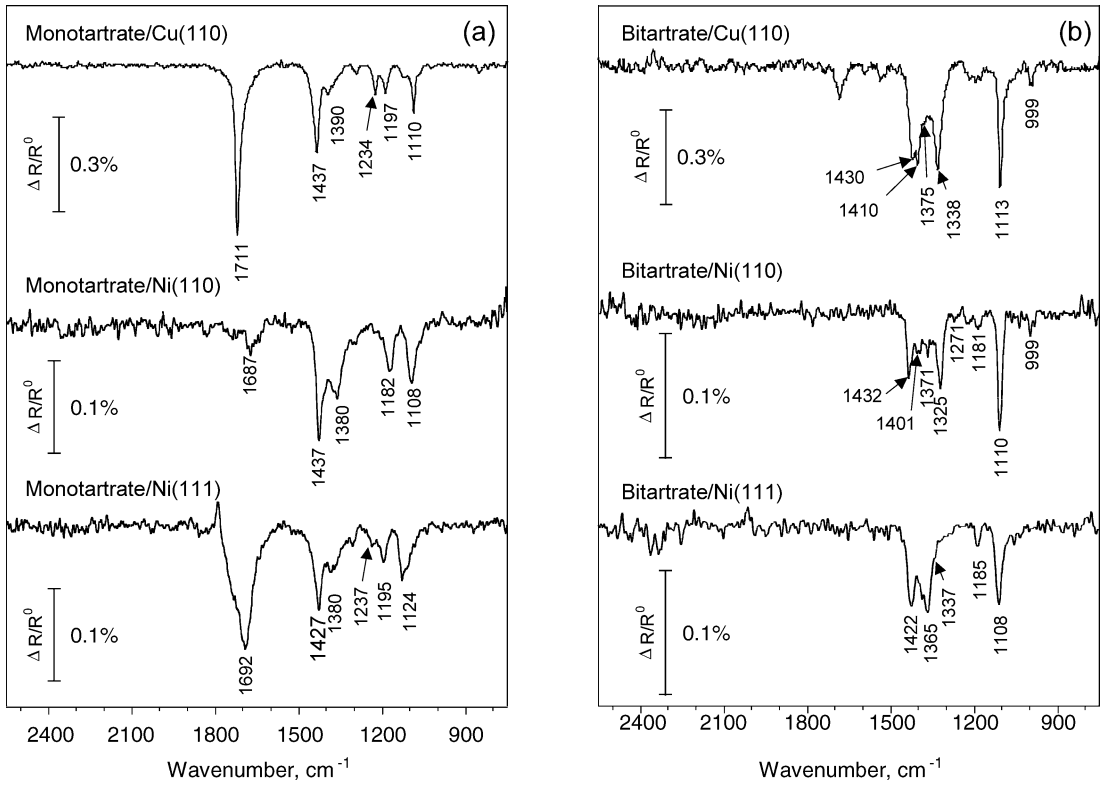

Fig. 4. (a) RAIR spectra collected for the monotartrate phase on Cu(110), Ni(110) and Ni(111). (b) RAIR spectra collected for the bitartrate phase on Cu(110), Ni(110), and Ni(111).

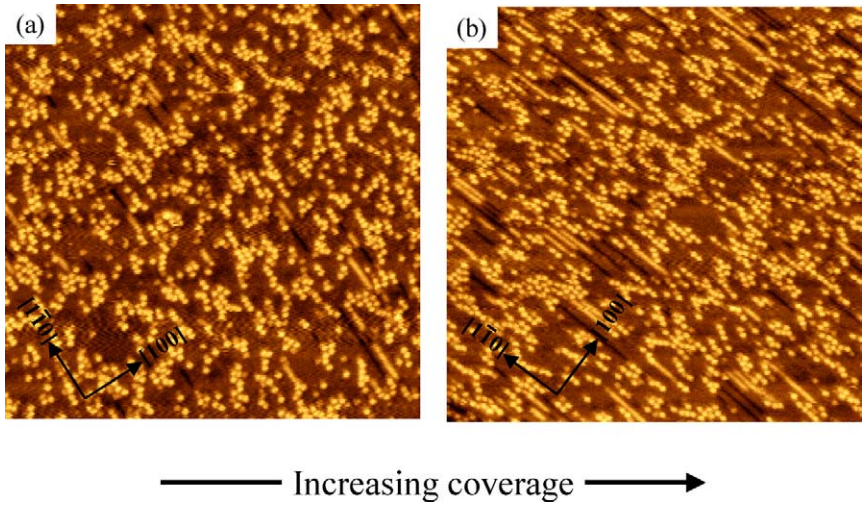

Fig. 5. STM images obtained with increasing coverage from (a) to (b) of the monotartrate form of (*R*,*R*)-tartaric acid adsorbed on Ni(110) at 170 K. (a to b) 500 × 500 Å, $V = -1.93$ V, $I = 1.0$ nA.

teristic biacid IR bands superimposed on the monotartrate signature (Figs. 3b and c).

3.4. Adsorption at 300 K: the bitartrate and monotartrate phases

Adsorption of (*R*,*R*)-tartaric acid on Ni(110) at 300 K leads to the creation of two different phases in the monolayer: the first consisting of the doubly deprotonated bitartrate species and the second containing only the monotartrate species (Fig. 1). Each phase is discussed separately below.

3.4.1. The bitartrate phase

RAIR spectra following increasing exposures of (*R*,*R*)-tartaric acid to Ni(110) at 300 K are shown in Fig. 6. At low coverage (Fig. 6a), the spectrum shows a complete absence of the $\nu_{C=O}$ band associated with the acid functionality. The carboxylate ν_{OCO}^{sym} vibration gives rise to two closely spaced

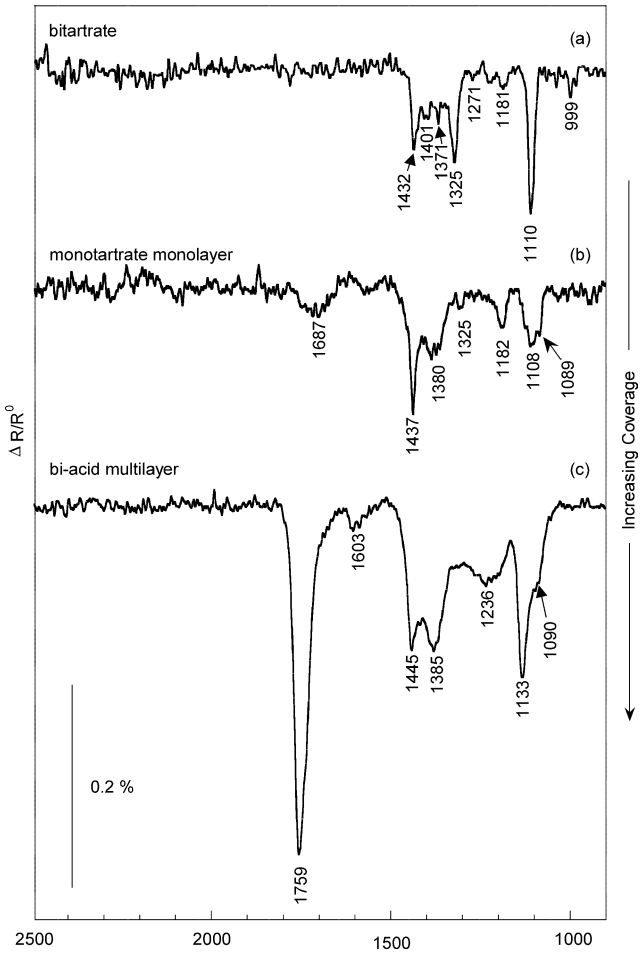

Fig. 6. RAIR spectra following the adsorption of (*R*,*R*)-tartaric acid on Ni(110) at 300 K as a function of coverage. Sublimation exposure time: (a) 6 min, (b) 9 min, and (c) 21 min.

small peaks at 1432 and 1401 cm^{-1}, which is a signature of the bitartrate system [13,14] and attributed to the coupling of the two COO-oscillators in the adsorbate. Changes are also seen for the 1325 and 1110 cm^{-1} peaks associated with the δ_{OH}^{alc} and ν_{C-OH}^{alc} vibrations, respectively, which both increase in relative intensity. A comparison of these values with IR data of tartrate salts [13,14], where the TA is present as bitartrate species (Table 1), provides a very good correlation. In addition, this spectrum possesses the same general characteristics exhibited by the bitartrate adsorbate on Cu(110) [5,20] and on Ni(111) as illustrated by Fig. 4b and the assignments in Table 1. Again, the appearance of only the symmetric component of the OCO stretch, ν_{OCO}^{sym}, and the absence of the asymmetric ν_{OCO}^{asym} vibration suggest that both oxygen atoms in each carboxylate group are approximately equidistant from the surface. However, the ν_{OCO}^{sym} is now even more strongly attenuated than in the monotartrate phase with a peak intensity of only 0.04%, which is almost 20 times lower in intensity than observed for the formate/Ni(110) system [22] where the OCO plane is held perpendicular to the metal surface. We, therefore, conclude that the OCO planes for both carboxylate groups are very strongly inclined toward the surface plane, presumably to enable both end functionalities to bond to the surface. This behaviour is similar to that observed for alanine [26] and glycine [27–30] on Cu(110) where the molecules straddle across the close-packed rows of the surface to achieve bonding via the both the carboxylate and the amine functionalities, thus forcing the OCO plane toward the surface.

No ordered overlayer LEED patterns were observed for this phase. STM data obtained at low exposures of (*R*,*R*)-tartaric acid to Ni(110) at room temperature to yield the bitartrate species are shown in Fig. 7. From these images, it can be seen that there are no long-range ordered structures of the type observed on Cu(110) [5,6], where highly ordered bitartrate chiral arrays aligned along a nonsymmetry direction are observed. Instead, initial adsorption (Figs. 7a and b) leads to random occupation of surface sites, with the creation of short 1-D molecular chains growing along the main <1–10> symmetry direction.

Periodic density functional theory (DFT) calculations on the bitartrate/Ni(110) phase, discussed in detail elsewhere [31], confirm that the bitartrate molecule is located above the 4-fold hollow site and bonds via both carboxylate groups, with each of the four oxygen atoms located at on-top sites, as depicted schematically within the phase diagram (Fig. 1). These studies also point out that the preferential adsorption site is located above the 4-fold hollow site [31]. Perhaps the most important aspect revealed by the DFT studies is that the bitartrate induces a significant relaxation of the metallic surface which not only forces the bonding pairs of Ni atoms 7.47 Å apart but also creates an asymmetric distortion in the Ni arrangement to describe an oblique, chiral footprint at the surface. In addition, the bitartrate molecule suffers a significant distortion in its backbone. Overall, the adsorption geometry also forces the OCO plane to be held just 38.5° away from the surface plane, explaining the largely attenuated intensity of the ν_{OCO}^{sym} vibration. The general structural conclusions of the DFT calculations are confirmed by detailed analysis of our STM images (Fig. 7c), where the molecular features in the STM images occupy, on average, a space of 6.8 × 4.6 Å, in good agreement with the calculated area of 7.04 × 4.98 Å [31] containing the relaxed bitartrate–Ni_4 complex. The STM images also reveal the presence of electronic distortions around the bitartrate molecules, extending, on average, over a 15.5 × 12.5 Å area for a single molecule, representing a 6 × 3.5 bulk truncation surface unit cell. These distortions are attributed to a local restructuring of the Ni atoms to relieve the stress induced by the large adsorption footprint, the resulting perturbation being propagated a number of atomic distances away from the adsorption centre. Finally, the presence of black troughs in the STM images is, again, due to H-induced reconstructions as discussed in the last section.

We note here that exploitation of the strict RAIRS dipole selection rules to deduce orientations of individual functional groups becomes invariably difficult when working with complex molecules, in particular for vibrations whose

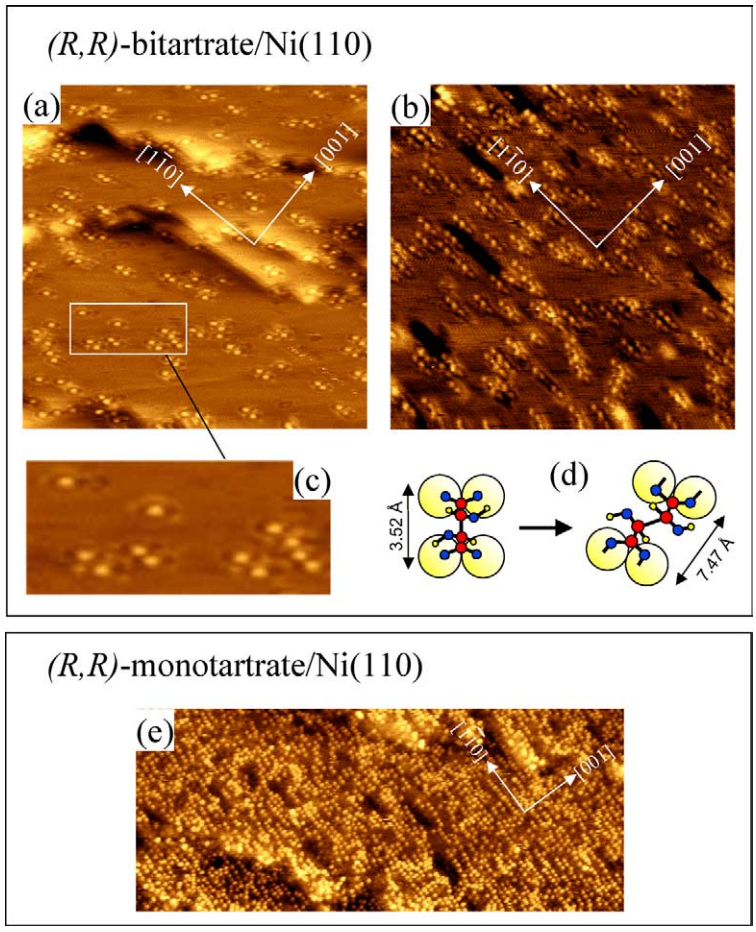

Fig. 7. STM images of (*R*,*R*)-tartaric acid adsorbed on Ni(110) at room temperature. (a) Low-coverage bitartrate phase, 300 × 300 Å, $V = -2.115$ V, $I = 1.16$ nA. (b) Medium coverage bitartrate phase, 300 × 300 Å, $V = -1.76$ V, $I = 1.0$ nA. (c) Enlarged picture of the bitartrate phase showing the molecular shape and surface perturbation, 45 × 100 Å, $V = -2.115$ V, $I = 1.16$ nA. (d) Schematic showing how the adsorption of the bitartarte species on the 4-fold bridging site on bulk Ni(110) leads to the distortion of both the molecule and the underlying metal atoms, which produce a chiral footprint at the surface. (e) High-coverage monotartrate species at room temperature, 300 × 750 Å, $V = -1.76$ V, $I = 1.0$ nA.

potential energy description is complex and involves a number of coupled motions. For example, the RAIRS orientation analysis of the COO– groups turns out to be largely correct since the amplitude of the vibration is largely concentrated within this functional group and the symmetric and asymmetric stretches lead to dipole moment changes in easily predictable directions. In contrast, simplistic analysis on the positioning of the C–OH groups at the chiral centres shows up unexpected discrepancies when compared to the structural model obtained by DFT. From the RAIR spectrum, the relative large intensity of the 1110 cm^{-1} peak associated with the ν^{alc}_{C-OH} vibration may lead one to surmise that the $C–O_{alcohol}$ bond is oriented toward the surface normal. However, the lowest energy configurations calculated by the DFT show the $C–O_{alcohol}$ bond almost parallel to the nickel surface. This discrepancy can be rationalised by the notion that the low-frequency vibration at 1110 cm^{-1} is not just restricted to a $C–O_{alcohol}$ stretch, but also involves a number of other coupled motions. Thus, the dynamic dipole moment change associated with this vibration may not necessarily align with the C–O bond direction, and so the RAIRS band intensity does not act as a reliable indicator of C–O bond orientation. This general viewpoint is also supported by recent calculations on polar charge distributions of the bitartrate–Ni_4 complex [32] clearly showing that the delocalised nature of the molecular wavefunctions leads to direct electronic communication between the molecule's chiral centres and its bonding groups. This not only leads to the transfer of chirality from the chiral centres to the bonding interactions [32] but also would lead vibrations at the chiral centres to induce dipole moment changes in the bonding groups that have a component normal to the surface.

3.4.2. *The monotartrate phase*

As a critical coverage is reached in the monolayer, the IR spectrum associated with the bitartrate form (Fig. 6b) disappears and is replaced by a spectrum which is very similar to that observed for the monotartrate form at low temperature (Fig. 3a). STM images obtained at high coverage in the monolayer (Fig. 7e) also show features that bear a close resemblance to those observed for the monotartrate phase at low temperatures (Fig. 5b). These changes clearly sug-

gest that the bitartrate phase created at room temperature converts into the monotartrate phase with increasing coverage, indicating that the bitartrate form is only preferred at low coverages, with the monotartrate being preferred at high coverages. These coverage-sensitive adsorbate preferences mimic those observed on Cu(110) [20] and lead to interesting kinetic phenomena, where the rates of adsorption and diffusion govern whether local islands with the critical coverage are nucleated leading to the creation of the monotartrate phase immediately upon exposure (as seen for Cu(110) for $T < 350$ K and as seen here on Ni(110) for $T < 300$ K) or whether lower density structures can be nucleated which lead to the bitartrate phase ($T > 350$ K for Cu(110), and $T \geqslant 300$ K, here, on Ni(110)). This aspect is also discussed by Jones and Baddeley for Ni(111) [9]. Of course, for those conditions in which the thermodynamically preferred route is followed, there remains the matter of converting the bitartrate into the monotartrate as the critical coverage is reached. For Cu(110), where no reservoir of hydrogen atoms exists at the surface at 300 K, this transformation is proposed to occur via proton transfer from incoming biacid molecules to the adsorbed bitartrate to give monotartrate in the following manner:

$$\underset{\text{adsorbed bitartrate}}{\text{OOCHOHCHOHCCOO(a)}} + \underset{\text{gas phase biacid}}{\text{HOOCHOHCHOHCCOOH(g)}} \rightarrow 2\ \underset{\text{adsorbed monotartrate}}{\text{OOCHOHCHOHCCOOH(a)}}.$$

On Ni(110), STM images show that presence of coadsorbed H, so a second route also opens up as:

$$\underset{\text{adsorbed bitartrate}}{\text{OOCHOHCHOHCCOO(a)}} + \underset{\text{adsorbed H}}{\text{H(a)}} \rightarrow \underset{\text{adsorbed monotartrate}}{\text{OOCHOHCHOHCCOOH(a)}}.$$

Finally, as the coverage is increased to multilayers (Fig. 6c), growth of the multilayer biacid over the monotartrate phase is observed.

4. Conclusions

A detailed study of the adsorption of (*R*,*R*)-tartaric acid on the defined Ni(110) surface was carried out as a function of temperature and coverage and shows that the local nature of the chiral adsorbate changes dynamically as conditions change. At very low temperatures of 90–120 K, the intact biacid molecular phase is the only form stabilised in both the monolayer and the multilayer regimes, with STM showing the random growth of molecular aggregate islands at the surface. In the temperature range 170–270 K, a very clear preference for the singly deprotonated monotartrate phase is observed over the entire monolayer coverage regime. This species is anchored to the nickel surface via its carboxylate functionality, while the opposite end remains intact as the acid group, with the vibration frequency of the $\nu_{C=O}$ stretch suggesting extensive H-bonding interactions. STM data show the presence of short molecular 1-D chains, with a preferred growth direction along the high symmetry <1–10> crystallographic axis. Adsorption at room temperature and above leads to coverage-dependent preferences in the monolayer: at low coverages, the doubly deprotonated bitartrate phase is preferred in which the adsorbate is strongly and rigidly anchored to the surface via both carboxylate groups; at increasing coverage, a dynamic change from the bitartrate species to the monotartrate species occurs. STM data of the bitartrate species do not show any long-range ordered structure of the type observed for Cu(110); instead, random occupation of the surface sites is observed, with a preferential growth of 1-D molecular chains directed along the main <1–10> crystallographic axis. Importantly significant electronic perturbations are imaged around the adsorbates, and DFT calculations show that the bitartrate adsorbate induces a chiral relaxation of atoms at the Ni(110) surface, in order to accommodate a large bitartrate–nickel$_4$ chiral footprint, thus causing a chirality transfer from the molecule into the metal. Overall, this work clearly demonstrates that the nature of the chiral modifier and, arguably, the most important dictator of enantioselective performance, is a dynamical function of adsorption conditions, and that an understanding of this is crucial for creating reproducible, highly enantioselective formulations.

Acknowledgments

We are grateful to the EPSRC for equipment grants and to BBSRC for a postdoctoral fellowship to V.H.

References

[1] Y. Izumi, Adv. Catal. 32 (1983) 215.
[2] G. Webb, P.B. Wells, Catal. Today 12 (1992) 319.
[3] M.A. Keane, G. Webb, J. Catal. 136 (1992) 1.
[4] A. Tai, T. Harada, Y. Hiraki, S. Murakami, Bull. Chem. Soc. Jpn. 56 (1983) 1414.
[5] M. Ortega Lorenzo, S. Haq, T. Bertrams, P. Murray, R. Raval, C.J. Baddeley, J. Phys. Chem. B 103 (1999) 10661.
[6] M. Ortega Lorenzo, C.J. Baddeley, C. Muryn, R. Raval, Nature 404 (2000) 376.
[7] R. Raval, C.J. Baddeley, S. Haq, S. Louafi, P. Murray, C. Muryn, M. Ortega Lorenzo, J. Williams, Stud. Surf. Sci. Catal. 122 (1999) 11.
[8] R. Raval, CATTECH 5 (2001) 12.
[9] T.E. Jones, C.J. Baddeley, Surf. Sci. 513 (2002) 453.
[10] V. Humblot, M. Ortega Lorenzo, C.J. Baddeley, S. Haq, R. Raval, J. Am. Chem. Soc. 126 (2004) 6460.
[11] S.M. Barlow, S. Louafi, D. Le Roux, J. Williams, C. Muryn, S. Haq, R. Raval, Langmuir 20 (2004) 7171.
[12] R. Bhattacharjee, Y.S. Jain, H.D. Bist, J. Raman Spectrosc. 20 (1989) 91.
[13] R. Bhattacharjee, Y.S. Jain, G. Raghubanshi, H.D. Bist, J. Raman Spectrosc. 19 (1988) 51.

[14] G.P. Srivastava, S. Mohan, Y.S. Jain, J. Raman Spectrosc. 13 (1982) 25.
[15] J.T. Edsall, J. Chem. Phys. 5 (1966) 508.
[16] R.G. Greenler, D.R. Snider, D. Witt, R.S. Sorbello, Surf. Sci. 118 (1982) 415.
[17] S. Haq, J.G. Love, D.A. King, Surf. Sci. 275 (1992) 170.
[18] T. Yuzawa, T. Higashi, J. Kubota, J. Kondo, K. Domen, C. Hirose, Surf. Sci. 325 (1995) 223.
[19] L.J. Bellamy, Advances in Infrared Group Frequencies, in: Methuen, 1968, p. 173.
[20] M. Ortega Lorenzo, V. Humblot, P. Murray, C.J. Baddeley, S. Haq, R. Raval, J. Catal. 205 (2002) 123.
[21] V. Humblot, C.J.A. Bingham, D. Le Roux, E. Mateo Marti, A. McNutt, T.S. Nunney, M. Ortega Lorenzo, A.J. Roberts, J. Williams, M. Surman, R. Raval, Surf. Sci. 537 (2003) 253.
[22] S. Haq, J.G. Love, H.E. Saunders, D.A. King, Surf. Sci. 325 (1995) 230.
[23] L.P. Nielsen, F. Besenbacher, E. Lægsgaard, I. Stensgaard, Rapid Commun. Phys. Rev. B 44 (1991) 13156.
[24] K. Christmann, F. Chehab, V. Penka, G. Ertl, Surf. Sci. 152 (1985) 256.
[25] V. Penka, K. Christmann, G. Ertl, Surf. Sci. 136 (1984) 307.
[26] J. Williams, S. Haq, R. Raval, Surf. Sci. 368 (1996) 303.
[27] N.A. Booth, D.P. Woodruff, O. Schaff, T. Giessel, R. Lindsay, P. Baumgärtel, A.M. Bradshaw, Surf. Sci. 397 (1998) 258.
[28] J. Hasselström, O. Karis, M. Weinelt, N. Wassdahl, A. Nilsson, M.G. Samant, J. Stöhr, Surf. Sci. 407 (1998) 221.
[29] S.M. Barlow, K. Kitching, S. Haq, N.V. Richardson, Surf. Sci. 401 (1998) 322.
[30] M. Nyberg, J. Hasselström, O. Karis, N. Wassdahl, M. Weinelt, A. Nilsson, L.G.M. Pettersson, J. Chem. Phys. 112 (2000) 5420.
[31] V. Humblot, S. Haq, C. Muryn, W.A. Hofer, R. Raval, J. Am. Chem. Soc. 124 (2002) 503.
[32] W.A. Hofer, V. Humblot, R. Raval, Surf. Sci. 554 (2004) 141.